

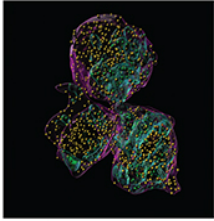


Title	Empagliflozin protects the kidney by reducing toxic ALB (albumin) exposure and preventing autophagic stagnation in proximal tubules
Author(s)	Matsui, Sho; Yamamoto, Takeshi; Takabatake, Yoshitsugu et al.
Citation	Autophagy. 2024, 21(3), p. 583-597
Version Type	VoR
URL	https://hdl.handle.net/11094/98359
rights	This article is licensed under a Creative Commons Attribution-NonCommercial-NoDerivatives 4.0 International License.
Note	

The University of Osaka Institutional Knowledge Archive : OUKA

<https://ir.library.osaka-u.ac.jp/>

The University of Osaka



Autophagy



ISSN: (Print) (Online) Journal homepage: www.tandfonline.com/journals/kaup20

Empagliflozin protects the kidney by reducing toxic ALB (albumin) exposure and preventing autophagic stagnation in proximal tubules

Sho Matsui, Takeshi Yamamoto, Yoshitsugu Takabatake, Atsushi Takahashi, Tomoko Namba-Hamano, Jun Matsuda, Satoshi Minami, Shinsuke Sakai, Hiroaki Yonishi, Jun Nakamura, Shihomi Maeda, Ayumi Matsumoto, Isao Matsui, Motoko Yanagita & Yoshitaka Isaka

To cite this article: Sho Matsui, Takeshi Yamamoto, Yoshitsugu Takabatake, Atsushi Takahashi, Tomoko Namba-Hamano, Jun Matsuda, Satoshi Minami, Shinsuke Sakai, Hiroaki Yonishi, Jun Nakamura, Shihomi Maeda, Ayumi Matsumoto, Isao Matsui, Motoko Yanagita & Yoshitaka Isaka (14 Oct 2024): Empagliflozin protects the kidney by reducing toxic ALB (albumin) exposure and preventing autophagic stagnation in proximal tubules, *Autophagy*, DOI: [10.1080/15548627.2024.2410621](https://doi.org/10.1080/15548627.2024.2410621)

To link to this article: <https://doi.org/10.1080/15548627.2024.2410621>



© 2024 The Author(s). Published by Informa UK Limited, trading as Taylor & Francis Group.



[View supplementary material](#)



Published online: 14 Oct 2024.



[Submit your article to this journal](#)



Article views: 707



[View related articles](#)



[View Crossmark data](#)

Empagliflozin protects the kidney by reducing toxic ALB (albumin) exposure and preventing autophagic stagnation in proximal tubules

Sho Matsui^a, Takeshi Yamamoto^a, Yoshitsugu Takabatake^a, Atsushi Takahashi^a, Tomoko Namba-Hamano^a, Jun Matsuda^a, Satoshi Minami^a, Shinsuke Sakai^a, Hiroaki Yonishi^a, Jun Nakamura^a, Shihomi Maeda^a, Ayumi Matsumoto^a, Isao Matsui^a, Motoko Yanagita^{b,c}, and Yoshitaka Isaka^a

^aDepartment of Nephrology, Osaka University Graduate School of Medicine, Osaka, Japan; ^bDepartment of Nephrology, Kyoto University Graduate School of Medicine, Kyoto, Japan; ^cInstitute for the Advanced Study of Human Biology, Kyoto University, Kyoto, Japan

ABSTRACT

The renoprotective effects of SLC5A2/SGLT2 (solute carrier 5 (sodium/glucose cotransporter), member 2) inhibitors have recently been demonstrated in non-diabetic chronic kidney disease (CKD), even without overt albuminuria. However, the mechanism underlying this renoprotection is largely unclear. We investigated the renoprotective mechanisms of the SLC5A2 inhibitor empagliflozin with a focus on ALB (albumin) reabsorption and macroautophagy/autophagy in proximal tubules using wild-type or drug-inducible *Lrp2/Megalin* or *atg5* knockout mice with high-fat diet (HFD)-induced obesity or 5/6 nephrectomy that elevated intraglomerular pressure without overt albuminuria. Empagliflozin treatment of HFD-fed mice reduced several hallmarks of lipotoxicity in the proximal tubules, such as phospholipid accumulation in the lysosome, inflammation and fibrosis. Empagliflozin, which decreases intraglomerular pressure, not only reduced the HFD-induced increase in ALB reabsorption *via* LRP2 in the proximal tubules (*i.e.* total nephron ALB filtration), as assessed by urinary ALB excretion caused by genetic ablation of *Lrp2*, but also ameliorated the HFD-induced imbalance in circulating ALB-bound fatty acids. Empagliflozin alleviated the HFD-induced increase in autophagic demand and successfully prevented autophagic stagnation in the proximal tubules. Similarly, empagliflozin decreased ALB exposure and autophagic demand in 5/6 nephrectomized mice. Finally, empagliflozin reduced HFD-induced vulnerability to ischemia-reperfusion injury, whereas LRP2 blockade and *atg5* ablation separately diminished this effect. Our findings indicate that empagliflozin reduces ALB exposure and prevents autophagic stagnation in the proximal tubules even without overt albuminuria. Autophagy improvement may be critical for the renoprotection mediated by SLC5A2 inhibition.

ARTICLE HISTORY

Received 17 March 2024
Revised 20 September 2024
Accepted
25 September 2024

KEYWORDS

Albuminuria; autophagic stagnation; lipotoxicity; LRP2/Megalin; lysosome; SLC5A2/SGLT2 inhibitors

Introduction

The prevalence of kidney disease is escalating worldwide, coinciding with the significant growth of aging populations and the emergence of obesity- and lifestyle-related disorders such as type 2 diabetes mellitus, dyslipidemia, and hypertension [1]. Despite the widespread use of renoprotective drugs such as renin-angiotensin-aldosterone system (RAAS) inhibitors, the incidence of chronic kidney disease (CKD) and subsequent progression to end-stage renal disease (ESRD) continues to increase. Therefore, preventing the development of CKD and delaying its progression to ESRD have been crucial objectives in the nephrology community.

SLC5A2/SGLT2 (solute carrier family 5 (sodium/glucose cotransporter), member 2) inhibitors, originally developed as hypoglycemic agents, have demonstrated potent renoprotective effects in patients with diabetic kidney disease (DKD) [2]. Furthermore, meta-analyses have suggested that SLC5A2 inhibitors also exhibit beneficial effects in preventing acute kidney

injury (AKI) [3,4]. Recent trials such as DAPA-CKD and EMPA-KIDNEY provided significant insights into the ability of SLC5A2 inhibitors to protect against non-diabetic CKD and advanced kidney disease, even without overt albuminuria [5,6]. Several mechanisms contribute to this improved renal prognosis, including a direct effect that reduces glucotoxicity and ATP consumption in SLC5A2-positive proximal tubules, a decrease in intraglomerular pressure resulting from restoration of tubuloglomerular feedback, and a diuretic effect [7,8]. It is generally accepted that one of the most important mechanisms is the suppression of glomerular hyperfiltration. Nevertheless, the precise mechanisms through which this confers renoprotection, even without overt albuminuria, remain unclear. Additionally, its impacts on the integrity of proximal tubular epithelial cells (PTECs) have not been fully elucidated.

ALB (albumin) filtered through glomeruli is reabsorbed primarily by the LRP2/megalin-CUBN (cubilin) receptor

CONTACT Takeshi Yamamoto  tyamamoto@kid.med.osaka-u.ac.jp 
S.Matsui. and T.Y. contributed equally to this work.

 Supplemental data for this article can be accessed online at <https://doi.org/10.1080/15548627.2024.2410621>

© 2024 The Author(s). Published by Informa UK Limited, trading as Taylor & Francis Group.
This is an Open Access article distributed under the terms of the Creative Commons Attribution-NonCommercial-NoDerivatives License (<http://creativecommons.org/licenses/by-nc-nd/4.0/>), which permits non-commercial re-use, distribution, and reproduction in any medium, provided the original work is properly cited, and is not altered, transformed, or built upon in any way. The terms on which this article has been published allow the posting of the Accepted Manuscript in a repository by the author(s) or with their consent.

complex lining the brush border of PTECs [9]. After endocytosis, ALB can undergo lysosomal degradation or transcytosis [10–12]. Recently, the quantitative roles of the glomerular filtration barrier and proximal tubule in the development of albuminuria have been reevaluated, and multiple lines of evidence now indicate that ALB filtration is more significant than previously thought [10]. Under normal physiological conditions, considerable amounts of plasma ALB pass through glomeruli and are reabsorbed in the S1–2 segments, resulting in undetectable albuminuria on urine dipsticks [13]. However, in the event of increased ALB filtration, the entire proximal tubule, including the S3 segment, participates in reabsorption, and albuminuria only develops when the capacity of all segments is exceeded [14]. Additionally, in the contexts of DKD, obesity, and lifestyle-related diseases, filtered ALB becomes more cytotoxic to PTECs exposed from the apical side, as ALB is modified by advanced glycation end products [15] and saturated fatty acids (FAs) [16,17]. These ALB-bound toxins could be absorbed *via* LRP2 into the PTECs and contribute to tubular damage, despite the absence or low levels of albuminuria on urine dipsticks [18,19].

Macroautophagy (hereafter autophagy) is a highly conserved intracellular degradation system that regulates homeostasis [20]. Recently, “autophagic stagnation” in PTECs has been identified as a common pathway for proximal tubular toxicity in various chronic conditions, including aging and obesity [16,21–23]. The basal autophagic activity is elevated in the kidneys of age- and obesity-related CKD, compared to control kidneys. However, autophagic activity cannot be sufficiently induced in response to additional stress. Mechanistically, age- and obesity-related stresses increase the “autophagic demand” (the amount of substrates requiring autophagic degradation to maintain cellular homeostasis), and “autophagic flux” (the actual degradation rate of autophagic substrates) rises in response to this heightened demand in the kidneys of age- and obesity-related CKD. Importantly, this increase in the autophagic demand does not always correlate with autophagic flux: autophagic flux is limited by the “autophagic capacity,” which is the maximum amount of intracellular substrates that autophagy can degrade. Thus, autophagic flux increases in parallel with the increase in autophagic demand only if the demand does not surpass the autophagic capacity; a prolonged increase in autophagic demand leads to sustained transport of autophagic substrates into lysosomes, resulting in lysosomal burden and dysfunction, which then impairs autophagic flux. To be clinically significant, it has recently been reported that increased autophagic demand is closely linked to the pathogenesis of Alzheimer’s disease: sustained autophagic demand results in autophagic stagnation due to lysosomal burden, exacerbating the disease’s progression [24]. In age- and obesity-related CKD, further autophagic activation, which would normally occur in response to additional stresses such as ischemia cannot be induced due to autophagic stagnation caused by a prolonged increase in autophagic demand [21,23]. Although several studies have shown that SLC5A2 inhibitors exert their protective effects by enhancing autophagy [25,26], these studies do not provide detailed insights into the mechanisms of SLC5A2 inhibitor-mediated autophagy activation.

On the basis of this information, we hypothesized that SLC5A2 inhibitors may alleviate autophagic stagnation in proximal tubules by modulating the quantity and quality of filtered ALB. We examined the renoprotective mechanisms of the SLC5A2 inhibitor empagliflozin, focusing on filtered ALB and the autophagy–lysosomal system in the proximal tubules of mouse models in which high-fat diet (HFD)-induced obesity or 5/6 nephrectomy caused elevated intraglomerular pressure without overt albuminuria.

Results

Empagliflozin reduces an HFD-induced phospholipid accumulation in the PTEC lysosomes

To investigate the therapeutic efficacy of empagliflozin against an HFD-induced phospholipid accumulation, eight-week-old wild-type mice were fed with a normal diet (ND) or HFD for 8 weeks, and HFD-fed mice were treated with vehicle or empagliflozin starting 6 weeks after initiation of the HFD. An HFD induced the development of cytosolic vacuoles in PTECs, most of which were colocalized with LAMP1 (lysosomal-associated membrane protein 1), and also led to the formation of dots positive for toluidine blue, which can detect not only lipid droplets but also phospholipids (Figure 1A) [27]. Similarly, in HFD-fed mice, PTECs exhibited many Nile red–positive dots, the majority of which were merged with LAMP1 (Figure 1B and S1A). These data suggest that an HFD induces the formation of enlarged lysosomes that contain phospholipids. Importantly, empagliflozin significantly decreased the number and size of these enlarged lysosomes, and also reduced phospholipid accumulation (Figure 1A–D). Electron microscopy revealed that empagliflozin diminished the HFD-induced formation of lamellar structures in lysosomes, which correspond to accumulated phospholipids (Figure 1E).

Moreover, we assessed lysosomal biogenesis and function in empagliflozin-treated HFD-fed mice. Lysosomal proteolytic activity, as assessed by protein levels of mature CTSB (cathepsin B) and mature CTSD (cathepsin D), showed no significant differences among ND-fed, HFD-fed, and empagliflozin-treated HFD-fed mice (Figure S1B). Lysosomal biogenesis, as assessed by protein levels of LAMP1, was increased in HFD-fed mice, which was attenuated by empagliflozin (Figure S1B). These results indicate that empagliflozin reduces lysosomal burden rather than increasing lysosomal function and biogenesis.

Furthermore, to investigate whether HFD-induced vacuole formation is caused by LRP2-mediated endocytosis, we used tamoxifen-inducible PTEC-specific *Lrp2*-deficient mice (*Lrp2*^{F/F}; *Ndrg1* [N-myc downstream regulated gene 1]-*CreERT2*, hereafter referred to as inducible *lrp2* knockout mice, iLrp2KO). Tamoxifen administration to ND-fed iLrp2KO mice decreased the protein levels of LRP2 and the mRNA levels of *Lrp2* (Figure S2A, S2B). Low-molecular-weight proteins such as RBP (retinol binding protein) and GC/VDBP (vitamin D binding protein) were detected in urine from tamoxifen-treated iLrp2KO mice but not from tamoxifen-treated *Lrp2*^{F/F} control mice (Figure S2C). Urinary ALB excretion increased to 220 ± 43 mg/day in tamoxifen-treated ND-fed iLrp2KO mice (Figure S2D), suggesting that a substantial amount of ALB that is filtered through the glomeruli is reabsorbed in the proximal tubules, even under

physiological conditions. Eight-week-old *Lrp2*^{F/F} control mice and iLRP2KO mice were fed an HFD for 8 weeks, and mice received tamoxifen to induce the genetic ablation of *Lrp2* 4 weeks after initiation of the HFD. Immunohistochemical analysis demonstrated HFD-induced vacuole formation in the PTECs of *Lrp2*^{F/F} control mice, but this formation was decreased in HFD-fed iLRP2KO mice (Figure S2E, S2F). Similarly, cilastatin, a known LRP2 blocker [28,29], suppressed HFD-induced vacuole formation in PTECs (Figure S2G). These data suggest that the vacuolar formation is LRP2-dependent, in agreement with a previous report.[30]

Empagliflozin alleviates kidney injury in CKD mice

To investigate the long-term consequences of empagliflozin treatment, we next monitored HFD-fed mice with or without empagliflozin for up to 10 months. Eight-week-old wild-type mice were fed a ND or HFD for 10 months, and HFD-fed mice were treated with vehicle or empagliflozin starting 5 months after initiation of the HFD. HFD induced tubulointerstitial fibrosis and ADGRE1/F4/80 (adhesion G protein-coupled receptor E1)-positive macrophage infiltration in the kidneys, and these were suppressed

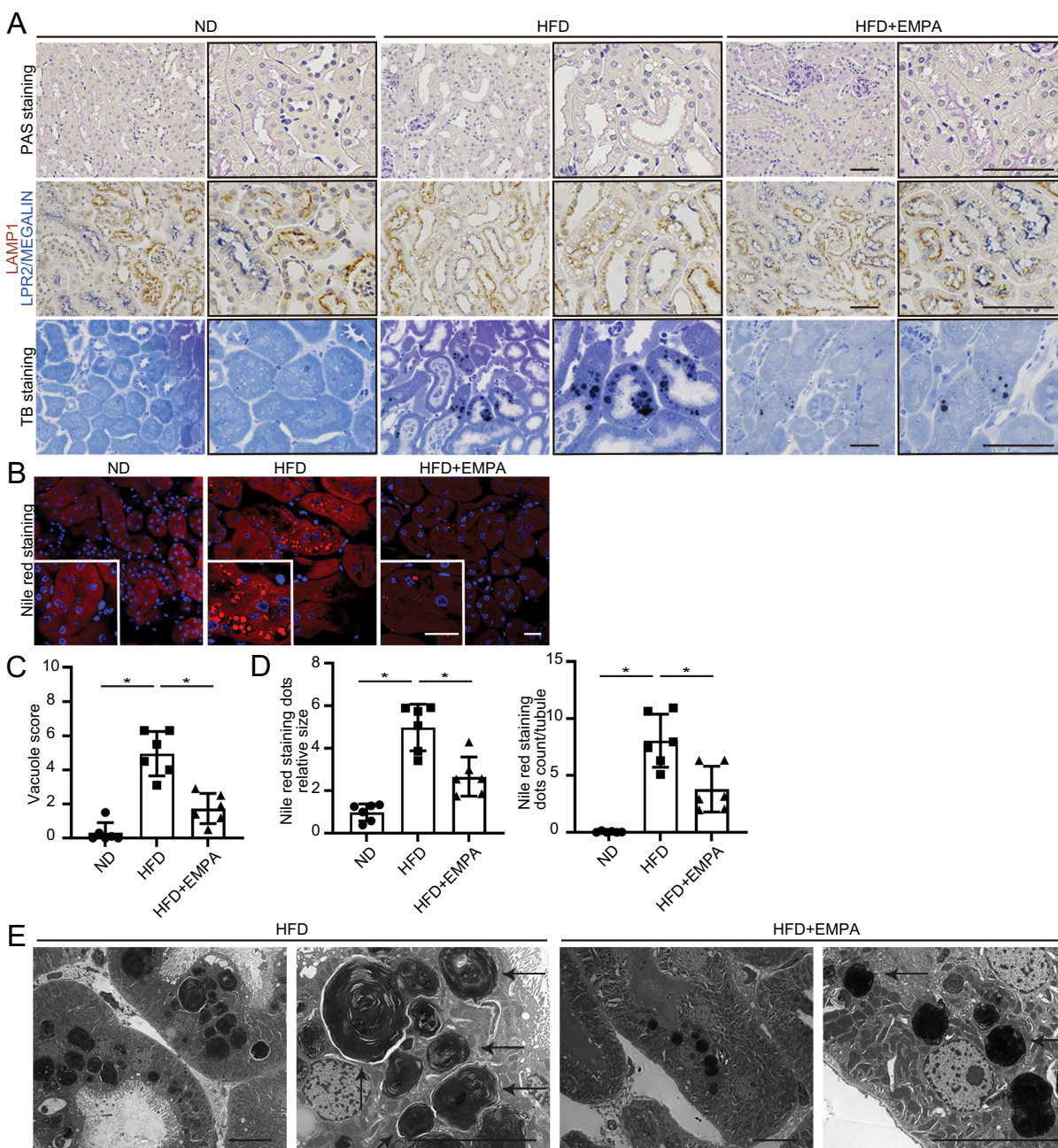


Figure 1. Empagliflozin reduces an HFD-induced phospholipid accumulation in the PTEC lysosomes. (A and B) Images of PAS staining, LAMP1 immunostaining, toluidine blue staining, and Nile red staining of the kidney cortical regions in ND-fed, HFD-fed, and empagliflozin (EMPA)-treated HFD-fed mice. Sections were coimmunostained for LRP2/MEGALIN, a marker of proximal tubules (blue) (A, middle) and counterstained with DAPI (blue) (B). (C and D) The vacuole scores from PAS staining images (C) and the relative sizes and number (per proximal tubule) of Nile red-positive puncta (D) are shown. The data in (D) were counted in at least 10 high-power fields ($\times 600$) (each high-power field contains 10–15 proximal tubules). (E) Electron micrographs of kidneys from the HFD-fed and EMPA-treated HFD-fed mice showing lamellar structures in lysosomes (arrow) ($n = 3$ in each group). Bars: 50 μm (A), 20 μm (B), 5 μm (E). Data are provided as means \pm SE. Statistically significant differences ($*p < 0.01$) are indicated. All images are representative of multiple experiments.

by empagliflozin (Figure 2A). Empagliflozin also alleviated HFD-induced renal dysfunction (Figure 2B, Figure S3A). Moreover, empagliflozin attenuated the increased oxidative stress in HFD-fed mice, as assessed by 4-hydroxy-2-nonenal (4HNE) and dityrosine (DT) (Figure 2C,D). We furthermore examined the renoprotective effect of empagliflozin against 5/6 nephrectomy-induced CKD, which manifests as low eGFR and renal fibrosis. [31] Eight-week-old wild-type mice were sham-operated or 5/6 nephrectomized, and 5/6 nephrectomized mice were treated with vehicle or empagliflozin for 6 weeks after nephrectomy. Empagliflozin reduced renal fibrosis, macrophage infiltration, oxidative stress, and improved renal function (Figure S3B-E). Collectively, empagliflozin alleviated kidney injury in CKD mice.

Empagliflozin alleviates total nephron ALB filtration and reabsorption

It is widely accepted that SLC5A2 inhibitors mitigate intraglomerular pressure. [32] To investigate whether empagliflozin reduces intraglomerular pressure in HFD-fed mice, we evaluated single-nephron glomerular filtration rate (SNGFR) using

in vivo imaging. [8] Eight-week-old wild-type mice were fed with a ND or HFD for 8 weeks, and HFD-fed mice were treated with vehicle or empagliflozin starting 6 weeks after initiation of the HFD, and the SNGFR was measured using multiphoton microscope. SNGFR in HFD-fed mice was significantly higher than in ND-fed mice, and this difference was reduced by empagliflozin (Figure 3A), indicating that empagliflozin could reduce intraglomerular pressure in HFD-fed mice.

Because filtered ALB is largely reabsorbed by LRP2, we propose to name urinary ALB excretion values in iLrp2KO mice as “total nephron ALB filtration”. Furthermore, “total nephron ALB reabsorption” can be calculated by subtracting urinary ALB excretion before tamoxifen from that after tamoxifen in iLrp2KO mice. We next evaluated the effect of empagliflozin on total nephron ALB filtration and reabsorption in iLrp2KO mice, using an HFD-induced obesity model in which intraglomerular pressure was increased in the absence of elevated blood glucose. [33] Eight-week-old iLrp2KO mice were fed a ND or HFD for 10 weeks, and HFD-fed mice were treated with vehicle or empagliflozin starting 6 weeks after initiation of the HFD; tamoxifen was then administered at 16 weeks of age; urine samples were collected before and 2 weeks after tamoxifen treatment. [34] There were no differences in urinary ALB levels between ND-fed, HFD-fed, and empagliflozin-treated HFD-fed

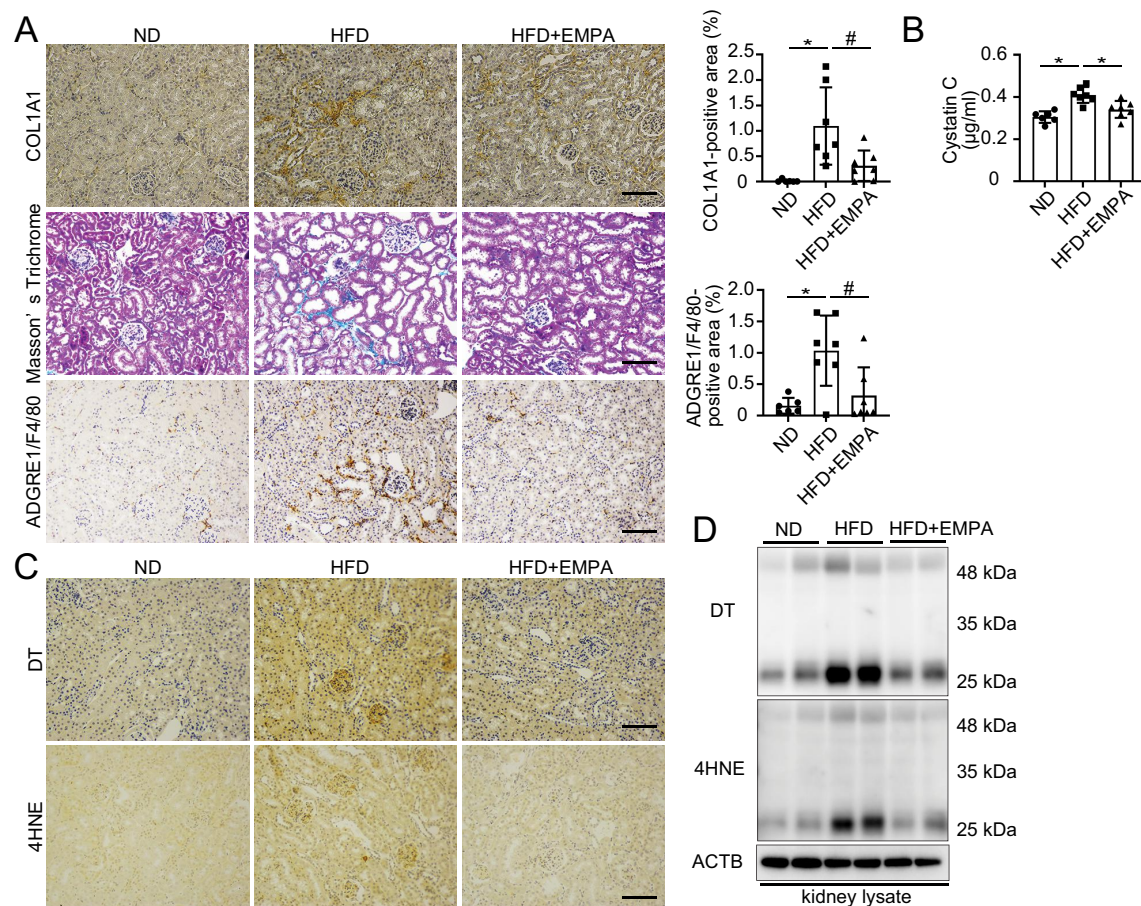


Figure 2. Empagliflozin alleviates kidney injury in HFD-induced CKD mice. (A) Images of COL1A1 immunostaining, Masson's trichrome staining, and ADGRE1/F4/80 immunostaining of kidney cortical regions in ND-fed, HFD-fed, and EMPA-treated HFD-fed mice ($n = 6-7$ in each group). COL1A1- or ADGRE1/F4/80-positive areas were quantified in at least 10 high-power fields ($\times 200$). (B) Plasma cystatin C levels of the mice in ND-fed, HFD-fed, and EMPA-treated HFD-fed mice. (C) Images of DT and 4HNE immunostaining of kidney cortical regions in ND-fed, HFD-fed, and EMPA-treated HFD-fed mice. (D) Western blots of DT and 4HNE in the kidneys of ND-fed, HFD-fed, and EMPA-treated HFD-fed mice. Bars: 100 μm (A, C). Data are provided as means \pm SE. Statistically significant differences ($*p < 0.01$, $\#p < 0.05$) are indicated. All images are representative of multiple experiments.

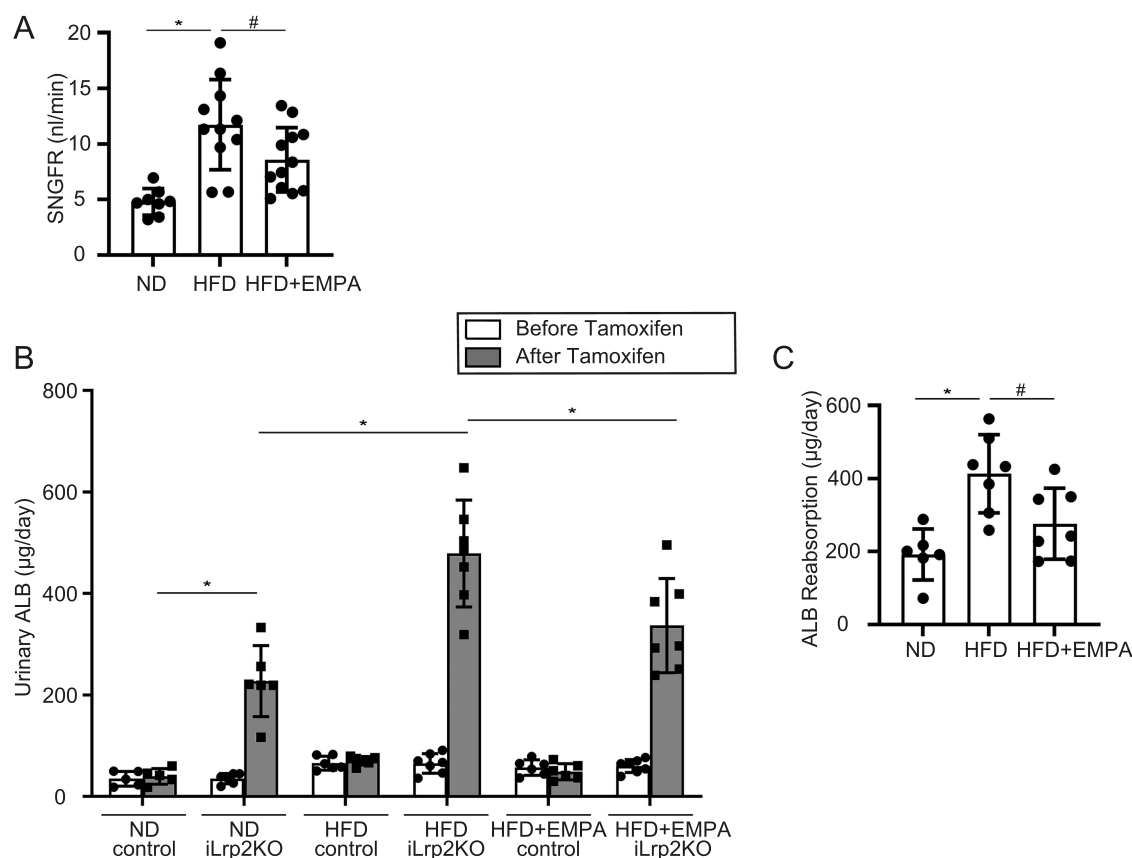


Figure 3. Empagliflozin alleviates the HFD-induced increase in total nephron ALB filtration and tubular ALB reabsorption. (A) The evaluation of SNGFR of ND-fed, HFD-fed, and EMPA-treated HFD-fed wild-type mice ($n = 8-12$ in each group). (B) The daily urinary ALB excretion of ND-fed, HFD-fed, and EMPA-treated HFD-fed iLrp2KO mice before tamoxifen and after tamoxifen ($n = 5-7$ in each group). Total nephron ALB filtration is estimated by urinary ALB excretion in iLrp2KO mice given tamoxifen. (C) The estimated tubular ALB reabsorption. Subtraction of ALB excretion before tamoxifen from that after tamoxifen corresponds to estimated tubular ALB reabsorption ($n = 6-7$ in each group). Data are provided as means \pm SE. Statistically significant differences ($*P < 0.01$, $\#P < 0.05$, N.S. not significant) are indicated.

iLrp2KO mice just before tamoxifen. By contrast, 2 weeks after tamoxifen treatment, we observed an increase in urinary ALB excretion (*i.e.*, total nephron ALB filtration) in HFD-fed iLrp2KO mice compared with ND-fed iLrp2KO mice, which was significantly decreased by empagliflozin (Figure 3B). Tubular ALB reabsorption was elevated in HFD-fed iLrp2KO mice compared with ND-fed iLrp2KO mice, which was suppressed in empagliflozin-treated HFD-fed iLrp2KO mice (Figure 3C). These data indicate that empagliflozin reduces total nephron ALB filtration and reabsorption *via* LRP2 in the proximal tubules in HFD-fed obese mice.

Empagliflozin decreases proximal tubule exposure to ALB, especially in S3 segments

To investigate the effect of empagliflozin on the fate of bovine serum albumin (BSA) filtered through the glomeruli, we performed an *in vivo* pulse-chase experiment using Alexa Fluor 555-conjugated BSA. When this compound was injected intravenously, its reabsorption was rarely detected in PTECs of iLrp2KO mice, indicating that filtered BSA was reabsorbed into the tubules *via* LRP2 (Figure S4A). Next, ND-fed, HFD-fed, and empagliflozin-treated HFD-fed mice were intravenously injected with Alexa Fluor 555-conjugated BSA. A greater number of Alexa

Fluor 555-positive dots was observed in all LRP2-positive proximal tubular segments of HFD-fed mice compared to ND-fed mice, and this difference was attenuated by empagliflozin (Figure 4A,B). Similarly, empagliflozin decreased proximal tubule exposure to ALB in 5/6 nephrectomized mice (Figure S4B, S4C).

Then, we evaluated how the effect of empagliflozin on ALB exposure differed between the SLC5A2-positive S1-2 and SLC5A2-negative S3 segments of PTECs (Figure 4C). Notably, in HFD-fed mice, empagliflozin had a more prominent impact on proximal tubule exposure to ALB in S3 segments than in S1-2 segments (Figure 4D,E). This indicates that in HFD-fed mice, the increase of glomerular ALB filtration could induce the incomplete ALB reabsorption in S1-2 segments and compensatory reabsorption in S3 segments, while empagliflozin may reduce the burden on S3 segments as well as S1-2 segments by decreasing glomerular ALB filtration.

Empagliflozin improves the metabolic status of HFD-fed mice

To investigate the effect of empagliflozin on the metabolic profiles of HFD-fed mice, 8-week-old wild-type mice were fed a ND or HFD for 8 weeks, and HFD-fed mice were treated with vehicle or empagliflozin starting 6 weeks after initiation

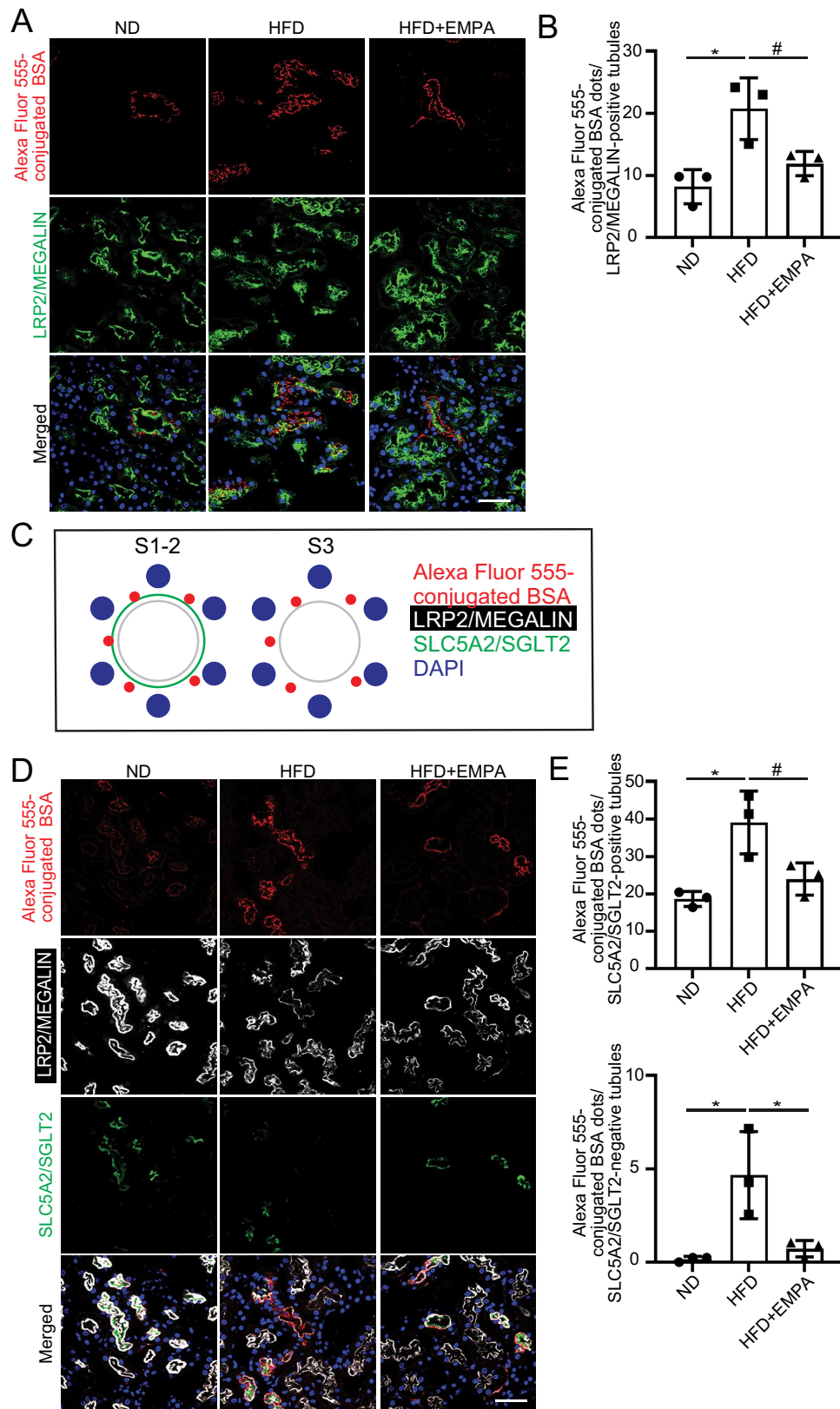


Figure 4. Empagliflozin decreases proximal tubule exposure to albumin, especially in S3 segments. (A) Kidney cortical regions of mice injected with Alexa Fluor 555-conjugated BSA (red) were stained with LRP2/MEGALIN (green) and counterstained with DAPI (blue). (B) The number of dots positive for Alexa Fluor 555-conjugated BSA was counted in LRP2/MEGALIN-positive proximal tubules ($n = 3$ in each group). (C) Schematic illustration of LRP2/MEGALIN and SLC5A2/SGLT2 staining patterns in the S1-2 and S3 segments of the proximal tubules. (D) Kidney cortical regions of ND-fed, HFD-fed, and EMPA-treated HFD-fed mice injected with Alexa Fluor 555-conjugated BSA (red) were stained with LRP2/MEGALIN (white) and SLC5A2/SGLT2 (green), and counterstained with DAPI (blue). (E) The numbers of dots positive for Alexa Fluor 555-conjugated BSA dots were counted in SLC5A2/SGLT2-positive (S1-2 segments) and -negative (S3 segments) proximal tubules ($n = 3$ in each group). Bars: 50 μm (A, D). Data are provided as means \pm SE. Statistically significant differences ($*p < 0.01$, $\# p < 0.05$) are indicated. All images are representative of multiple experiments.

of the HFD. Data are shown in Table 1. Empagliflozin reduced plasma levels of cholesterol, triglycerides, and phospholipids, but there were no significant changes in blood pressure, blood glucose, or body weight (Table 1 and Figure 5A). Interestingly, empagliflozin significantly decreased white adipose tissue mass in the viscera but not the epididymis (Table 1). Empagliflozin attenuated the increases in cell size and number of infiltrating macrophages (detected as crown-like structures) in the visceral fat of HFD-fed mice (Figure 5B,C). In addition, to assess changes in FA composition in detail, we measured plasma levels of 24 FA fractions (Table 2). Plasma levels of saturated and monounsaturated FAs were increased and decreased, respectively, in HFD-fed mice, with no changes seen following empagliflozin treatment. Notably, empagliflozin ameliorated the HFD-induced decreases in n3-polyunsaturated fatty acids (PUFAs), such as docosapentaenoic acid and docosahexaenoic acid, which are known to reduce the incidence of cardiovascular events (Table 2). [35] Collectively, empagliflozin

ameliorated the HFD-induced imbalance in circulating FAs bound to ALB, suggesting that empagliflozin may improve the lipoquality of reabsorbed ALB.

Empagliflozin reduces autophagic demand in PTECs

Next, we explored the mechanism whereby empagliflozin achieves a renoprotective effect by decreasing proximal tubule exposure to ALB (*i.e.*, ALB reabsorption *via* LRP2) and improving the systemic metabolic state. We focused on autophagy because HFD-induced obesity burdens the lysosomal system, leading to autophagic stagnation in PTECs. [16,21] First, we investigated the effect of empagliflozin on the HFD-induced increase in autophagic demand, using tamoxifen-inducible PTEC-specific autophagy-deficient mice (*Atg5^{F/F}*; *Ndr1-CreERT2*, hereinafter referred to as inducible *atg5* knockout mice, *iAtg5KO*). Eight-week-old *Atg5^{F/F}* control and *iAtg5KO* mice were fed a ND or HFD for 11 weeks, and HFD-fed mice were treated with vehicle or empagliflozin starting 6 weeks after initiation of the HFD. Three weeks before euthanasia, mice

Table 1. Metabolic profiles of ND-fed, HFD-fed, and empagliflozin-treated HFD-fed mice.

Characteristic	ND	HFD	HFD+EMPA
Food intake (kcal/day)	12.2 ± 0.4	15.0 ± 0.9 ^a	15.0 ± 0.7 ^a
Systolic blood pressure (mmHg)	93.1 ± 4.8	91.7 ± 4.1	97.6 ± 3.2
Kidney (mg)	167.3 ± 4.3	183.8 ± 10.7	169.8 ± 3.4
Liver (mg)	1226.3 ± 64.2	1512.1 ± 122.1 ^a	1117.9 ± 51.2 ^b
Visceral white adipose tissue (mg)	340.0 ± 47.2	1125.1 ± 211.0 ^a	651.8 ± 110.5 ^b
Epididymal white adipose tissue (mg)	702.3 ± 91.7	2479.6 ± 322.7 ^a	2443.8 ± 347.5 ^a
Plasma total cholesterol (mM)	2.47 ± 0.07	4.41 ± 0.29 ^a	3.96 ± 0.30 ^a
Plasma triglycerides (mM)	0.89 ± 0.08	1.56 ± 0.14 ^a	1.15 ± 0.10 ^b
Plasma phospholipids (mM)	2.43 ± 0.23	3.26 ± 0.16 ^a	2.47 ± 0.11 ^b

Metabolic profiles were analyzed in the ND-fed, HFD-fed, and empagliflozin-treated HFD-fed mice ($n = 6$ in each group). a, $p < 0.05$ vs ND; b, $p < 0.05$ vs HFD in each corresponding group.

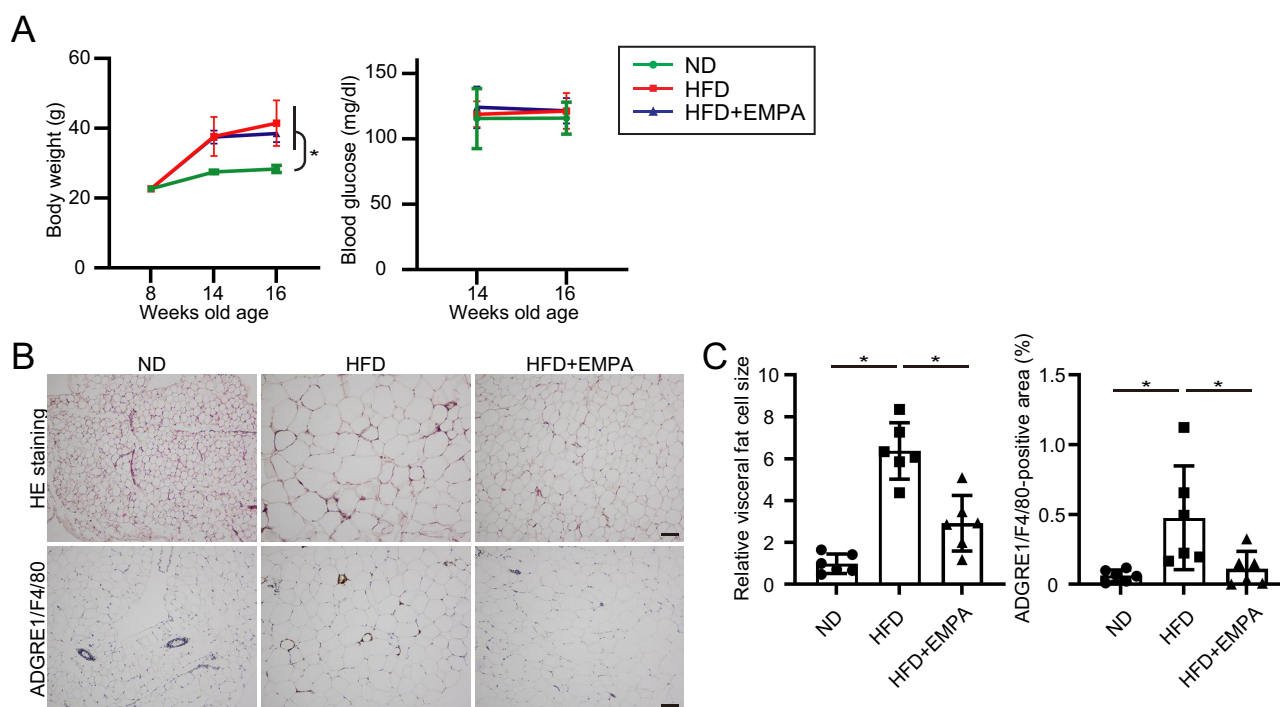


Figure 5. Empagliflozin improves the metabolic status of HFD-fed mice. (A) Changes in body weight and blood glucose levels during the experimental period. (B) Images of HE staining and ADGRE1/F4/80 immunostaining of visceral white adipose tissue ($n = 6$ in each group). (C) The relative cell size and ADGRE1/F4/80-positive area were quantified in at least 5 high-power fields ($\times 100$). Bars: 100 μm (B). Data are provided as means \pm SE. Statistically significant differences ($*p < 0.01$, $\#p < 0.05$, N.S. not significant) are indicated. All images are representative of multiple experiments.

Table 2. Plasma levels of 24 FA fractions in ND-fed, HFD-fed, and empagliflozin-treated HFD-fed mice.

	free fatty acids	ND	HFD	HFD+EMPA
saturated fatty acid	lauric acid (µg/ml)	0.52 ± 0.06	0.40 ± 0.03	0.40 ± 0.03
	myristic acid (µg/ml)	8.4 ± 1.2	6.5 ± 0.5	6.6 ± 0.2
	palmitic acid (µg/ml)	498.4 ± 27.1	572.1 ± 16.3 ^a	617.9 ± 13.4 ^a
	stearic acid (µg/ml)	173.7 ± 8.0	366.5 ± 13.8 ^a	363.4 ± 23.1 ^a
	arachidic acid (µg/ml)	7.0 ± 0.6	8.0 ± 0.4	8.7 ± 0.1 ^a
	lignoceric acid (µg/ml)	5.4 ± 0.8	4.6 ± 0.5	4.9 ± 0.1
monounsaturated fatty acid	behenic acid (µg/ml)	10.1 ± 0.7	21.4 ± 0.9 ^a	25.8 ± 0.1 ^{ab}
	myristoleic acid (µg/ml)	0.6 ± 0.11	0.36 ± 0.09 ^a	0.36 ± 0.02 ^a
	palmitoleic acid (µg/ml)	64.6 ± 10.8	32.8 ± 1.6 ^a	30.5 ± 1.3 ^a
	oleic acid (µg/ml)	335.3 ± 26.1	380.8 ± 26.7	388.7 ± 20.3
	eikosenoic acid (µg/ml)	11.6 ± 0.6	5.8 ± 0.5 ^a	5.1 ± 0.8 ^a
	5-8-11eikosatrienic acid (µg/ml)	2.8 ± 0.4	9.9 ± 0.6 ^a	7.6 ± 0.5 ^{ab}
	erucic acid (µg/ml)	1.5 ± 0.2	<1.0	<1.0
	nervonic acid (µg/ml)	11.9 ± 0.2	9.4 ± 0.3 ^a	8.8 ± 0.8 ^a
<i>n</i> -6 polyunsaturated fatty acid	linoleic acid (µg/ml)	675.4 ± 25.6	704.5 ± 28.2	783.8 ± 26.7 ^a
	γ-linolenic acid (µg/ml)	7.9 ± 0.7	11.3 ± 0.8 ^a	13.6 ± 0.5 ^{ab}
	docosatetraenoic acid (µg/ml)	2.7 ± 0.1	5.9 ± 0.2 ^a	5.8 ± 0.2 ^a
	arachidonic acid (µg/ml)	189.7 ± 7.9	626.3 ± 59.9 ^a	628.7 ± 70.0 ^a
	dihomo-γ-linolenic acid (µg/ml)	37.5 ± 2.9	47.8 ± 7.2	36.0 ± 4.1
	eikosazienoic acid (µg/ml)	5.9 ± 0.2	6.2 ± 0.4	5.82 ± 0.2
<i>n</i> -3 polyunsaturated fatty acid	docosapentaenoic acid (µg/ml)	13.54 ± 0.98	8.64 ± 0.20 ^a	10.54 ± 0.30 ^{ab}
	eicosapentaenoic acid (µg/ml)	44.5 ± 3.8	14.1 ± 1.1 ^a	14.5 ± 1.6 ^a
	docosahexaenoic acid (µg/ml)	194.1 ± 6.3	203.6 ± 8.3	249.9 ± 8.8 ^{ab}
	α-linolenic acid (µg/ml)	11.8 ± 0.7	5.7 ± 0.5 ^a	6.5 ± 0.3 ^a

Plasma levels of 24 FA fractions were analyzed in the ND-fed, HFD-fed, and empagliflozin-treated HFD-fed mice ($n = 5$ in each group). a, $p < 0.05$ vs ND; b, $p < 0.05$ vs HFD in each corresponding group.

received tamoxifen to induce the genetic ablation of *Atg5* (Figure S5A). The accumulation of SQSTM1/p62 (sequestosome 1) and ubiquitin represents the amount of substrate requiring degradation during the preceding 3-week period. The ablation of autophagy triggered more accumulation of SQSTM1/p62- and ubiquitin-positive protein aggregates in HFD-fed *iAtg5KO* mice than in ND-fed *iAtg5KO* mice. Notably, the accumulation of autophagy substrates was decreased by empagliflozin in HFD-fed *iAtg5KO* mice (Figure 6A). The protein levels of proteasome 20S $\alpha\beta$ were not increased by empagliflozin (Figure S5B), suggesting that SQSTM1/p62 and ubiquitin could be evaluated as autophagy substrates. Similar to HFD-fed mice, empagliflozin decreased autophagic demand in the PTECs of 5/6 nephrectomized mice (Figure S5C). Collectively, empagliflozin attenuated the increased autophagic demand in the PTECs of mouse models with hyperfiltration.

Empagliflozin alleviates autophagic stagnation in PTECs

Next, we investigated whether empagliflozin can restore autophagic flux in the kidney of HFD-fed mice. To evaluate how basal and starvation-induced autophagic flux was altered by empagliflozin, we used GFP-MAP1LC3B (green fluorescent protein-microtubule-associated protein 1 light chain 3 beta) transgenic mice. Chloroquine, an inhibitor of intralysosomal acidification, was administered 6 hours before euthanasia, and the number of GFP-positive puncta (which represent autophagosomes) was compared with and without chloroquine administration. [22] As we previously reported, [16] the PTECs in ND-fed mice exhibited low basal autophagic activity and high levels of starvation-induced autophagy, while those in HFD-fed mice exhibited high basal autophagic activity with autophagic stagnation in response to starvation. Notably, empagliflozin lowered basal autophagic activity, probably due to reduced autophagic demand, and successfully restored autophagic flux during starvation (Figure 6B). Western blot analysis (MAP1LC3-I,

MAP1LC3-II and SQSTM1/p62) using whole kidney lysates (Figure S6) confirmed this fluorescent study.

Empagliflozin reduces HFD-induced vulnerability to Ischemia-reperfusion (IR) injury in an autophagy-dependent manner

Although there is still concern that SLC5A2 inhibitors may increase the risk of AKI caused by hemodynamic mechanisms, clinical trials have shown that the incidence of AKI is rather low. Moreover, we observed that empagliflozin reduced ALB exposure, especially in S3 segments, which are susceptible to ischemia. Therefore, we subjected mice to IR injury to determine whether autophagic flux restored by empagliflozin could reduce HFD-induced vulnerability to ischemic stress, because autophagy has a protective role against IR injury. Severe tubular injury characterized by abundant sediment was observed in IR-injured HFD-fed *Atg5^{F/F}* control mice, and this injury was attenuated in empagliflozin-treated HFD-fed *Atg5^{F/F}* control mice (Figure 7A, C). The number of terminal deoxynucleotidyl transferase dUTP nick end labeling (TUNEL)-positive tubular cells after IR injury was significantly decreased in empagliflozin-treated HFD-fed *Atg5^{F/F}* control mice compared to HFD-fed *Atg5^{F/F}* control mice (Figure 7B,D). The protein levels of SQSTM1/p62 were increased in IR-injured kidneys of HFD-fed *Atg5^{F/F}* control mice, and this increase was attenuated in empagliflozin-treated HFD-fed *Atg5^{F/F}* control mice, indicating that empagliflozin prevents HFD-induced autophagic stagnation during ischemic AKI (Figure S7A). However, the protective effect of empagliflozin was diminished by autophagy deficiency (Figure 7A–D). The mRNA levels of the tubular injury marker *Havcr1/Kim-1* and HAVCR1/KIM1-positive tubules paralleled the tubular injury score (Figure 7E,F). Similarly, we used IR-injured mice to determine whether reduced reabsorption of toxic ALB by empagliflozin could reduce HFD-induced vulnerability to ischemic

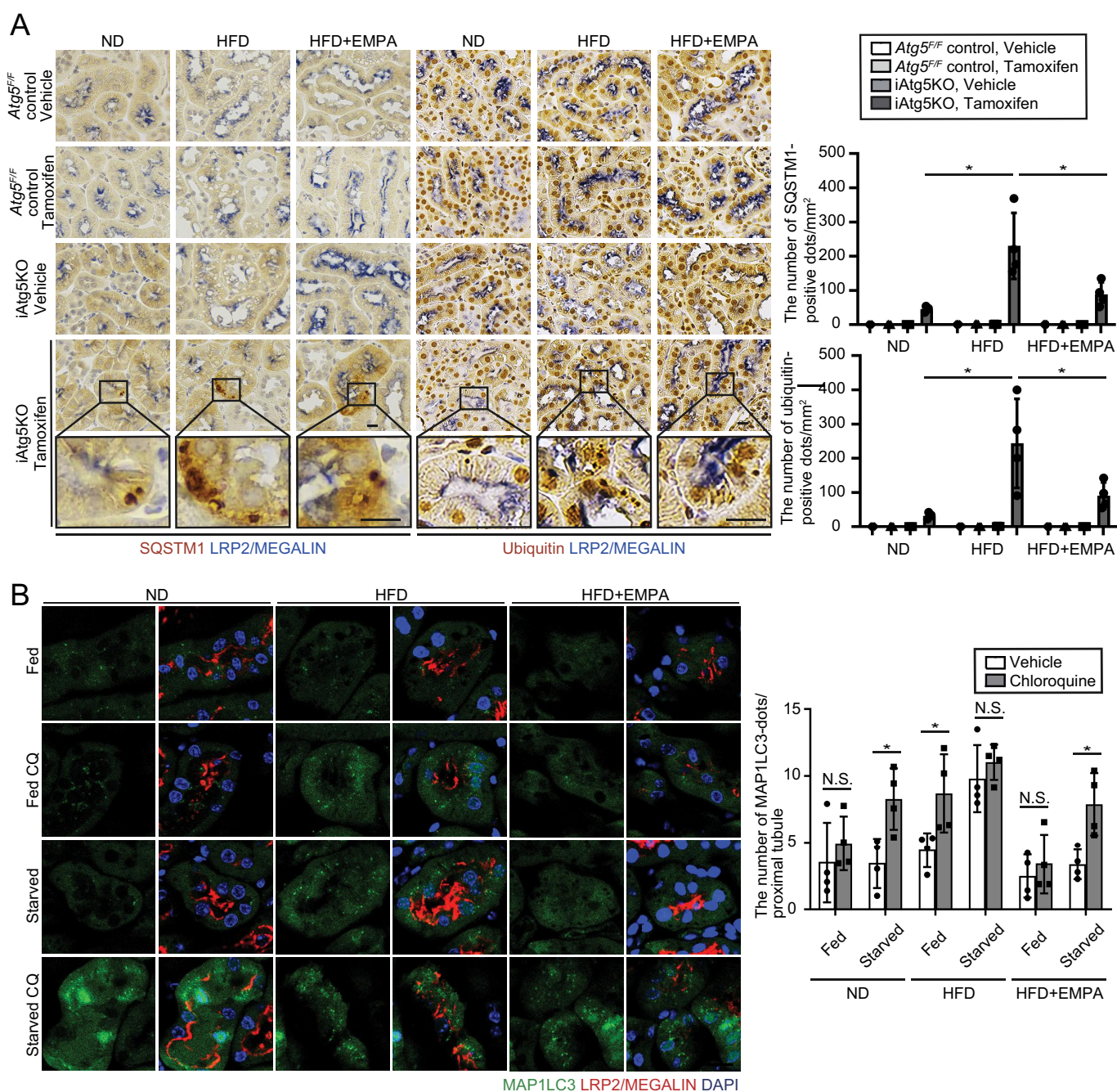


Figure 6. Empagliflozin alleviates the HFD-induced increase in autophagic demand and prevents autophagic stagnation in the proximal tubules. (A) Kidney cortical regions of ND-fed, HFD-fed, and EMPA-treated HFD-fed (*Atg5^{FF}* control and *iAtg5KO*) mice were immunostained for SQSTM1/p62 and ubiquitin after treatment with vehicle or tamoxifen 3 weeks before euthanasia ($n = 4-5$ in each group). Sections were coimmunostained for LRP2/MEGALIN, a marker of proximal tubules (blue). Magnified images from the tamoxifen-treated *iAtg5KO* mice are also presented. The number of SQSTM1/p62- or ubiquitin-positive dots was counted in at least 10 high-power fields ($\times 400$). (B) GFP-positive puncta formation was assessed in the proximal tubules of ND-fed, HFD-fed, and EMPA-treated HFD-fed GFP-MAP1LC3 transgenic mice that were either fed a ND or HFD diet or subjected to 24 h of starvation, with or without chloroquine (CQ) administration 6 h before euthanasia. Kidney sections were immunostained for LRP2/MEGALIN (red), and counterstained with DAPI (blue). The number of GFP-positive puncta per proximal tubule under each condition was counted in at least 10 high-power fields (original magnification, $\times 600$) (each high-power field contained 10–15 proximal tubules). Bars: 10 μm (A, B). Data are provided as means \pm SE. Statistically significant differences ($*p < 0.01$, N.S. not significant) are indicated. All images are representative of multiple experiments. CQ, chloroquine.

stress. Cilastatin was administered to block ALB reabsorption *via* LRP2. Empagliflozin exhibited protective effects in vehicle-treated HFD-fed mice (Figure S7B–G), and these were abrogated by the cilastatin-mediated blockade of LRP2. These data suggest that empagliflozin counteracts kidney injury at least partly by decreasing proximal tubule exposure to ALB and improving autophagy.

Discussion

In this study, we elucidated the mechanisms underlying empagliflozin's renoprotective effects even in conditions without overt albuminuria. Mechanistically, empagliflozin not only ameliorates metabolic dysfunction but also reduces proximal tubule exposure to ALB (*i.e.*, filtered ALB that should be reabsorbed *via*

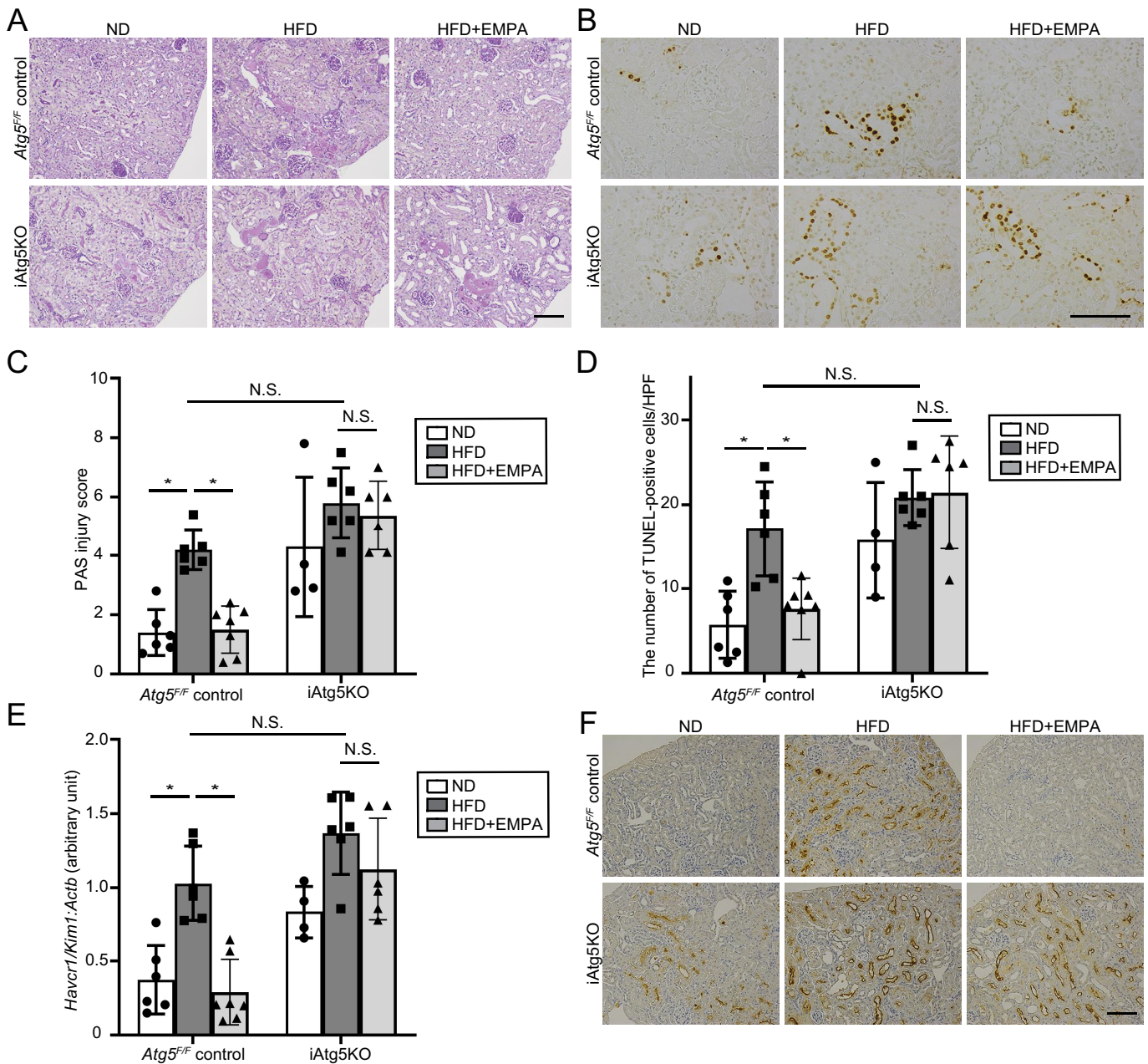


Figure 7. Empagliflozin reduces HFD-induced vulnerability to IR injury in HFD-fed mice in an autophagy-dependent manner. (A, B) Images of PAS (A) and TUNEL (B) staining of kidney cortexes from ND-fed, HFD-fed, and EMPA-treated HFD-fed *Atg5^{FF}* control and *iAtg5KO* mice 2 days after a unilateral IR injury ($n = 4-7$ in each group). (C) The PAS injury score is shown. (D) The number of TUNEL-positive PTECs was calculated in at least 10 high-power fields ($\times 200$). (E, F) The mRNA levels of *Havcr1/Kim1* (E), and the representative images of immunostaining for HAVCR1/KIM1 (F) in ND-fed, HFD-fed, and EMPA-treated HFD-fed *Atg5^{FF}* control and *iAtg5KO* mice 2 days after a unilateral IR injury. Bars: 100 μm (A, B, F). Data are provided as means \pm SE. Statistically significant differences ($*p < 0.01$, $\#p < 0.05$, N.S. not significant) are indicated. All images are representative of multiple experiments.

LRP2 in proximal tubules) even in conditions without overt albuminuria. Empagliflozin alleviated autophagic demand, ameliorated lysosomal phospholipid accumulation and autophagic stagnation. Consequently, empagliflozin reduced the vulnerability to ischemia-reperfusion injury in conjunction with the LRP2-autophagy axis. A schematic diagram illustrating these mechanisms is presented in Figure 8.

We performed *in vivo* experiments designed to specifically investigate the effects of SLC5A2 inhibition on the proximal tubules in non-diabetic models with elevated intraglomerular pressure in the absence of overt albuminuria. Overall, the

renoprotective effects of empagliflozin were consistent and significant in our models. Furthermore, LRP2 blockade and ablation of proximal tubular autophagy showed that these effects were dependent on the effects of LRP2 and autophagy, probably due to upstream improvement in glomerular hemodynamics. Our findings may explain the essential mechanism underlying renoprotection mediated by SLC5A2 inhibition, not only in albuminuric DKD but also in nonalbuminuric advanced CKD, as recently reported in the EMPA-KIDNEY trial [6].

Among the theories explaining SLC5A2 inhibition-mediated renoprotection, one based on glomerular

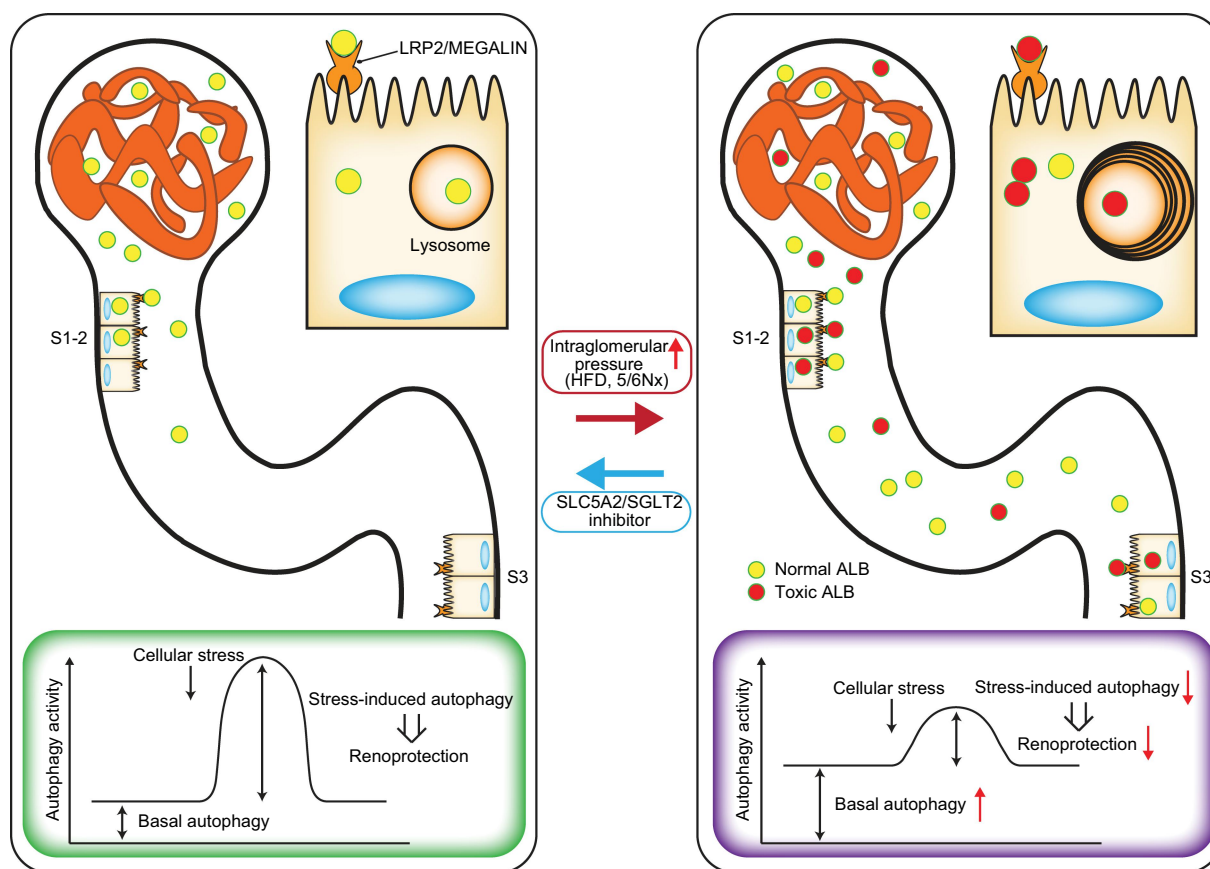


Figure 8. Schematic illustration of this study. Increased glomerular pressure caused by HFD or 5/6 nephrectomy induces tubular reabsorption of toxic ALB *via* LRP2, leading to increased autophagic demand and stagnation of autophagy flux, which can increase vulnerability to IR injury. Empagliflozin reduces intraglomerular pressure and ameliorates metabolic dysfunctions, thereby improving the quantity and quality of filtered ALB and alleviating autophagic stagnation in PTECs. This prevention of autophagic stagnation can eventually improve the integrity of PTECs, thus leading to renoprotection.

hemodynamics is the most well developed and widely accepted. There is mounting evidence that SLC5A2 inhibition mitigates hyperfiltration by reducing the reabsorption of fluid and NaCl by the proximal tubules, thereby evoking a tubuloglomerular feedback response [7,8]. Indeed, we revealed that empagliflozin reduced ALB reabsorption *via* LRP2 in the proximal tubules (*i.e.*, total nephron ALB filtration) in mouse models of increased intraglomerular pressure. From the viewpoint of reducing hyperfiltration, RAAS inhibitors and SLC5A2 inhibitors may share similar anti-albuminuric mechanisms. However, we found that empagliflozin improved several aspects of metabolic syndrome, including the quality of FAs bound to circulating ALB, especially *n*-3 PUFAs such as docosahexaenoic acid. Notably, toxic ALB that is transported to lysosomes undergoes lysosomal degradation, which may burden lysosomes, while most reabsorbed nontoxic ALB undergoes tubular transcytosis and is recycled [10,12]. Empagliflozin's ability to improve the quality of filtered ALB may therefore prove pivotal in distinguishing it from RAAS inhibitors.

A reduction in ALB reabsorption *via* LRP2 may play a key role in the protective function of empagliflozin. The contribution of LRP2 to the development of tubulointerstitial injury or AKI is still a controversial matter [36,37]. Nonetheless, accumulating evidence suggests that LRP2 is involved in the progression of CKD [38–40], and genetic LRP2 ablation

ameliorates tubular lysosomal overload in HFD-induced obesity and nephropathic cystinosis, supporting an endocytosis-based mechanism [30,34,41]. Therefore, pharmacological LRP2 blockade is a promising method for preventing kidney injury [29,41,42]; however, its long-term side effects remain unknown, which is an important consideration given that LRP2 reabsorbs essential molecules. Empagliflozin was able to reduce ALB reabsorption without LRP2 blockade by reducing glomerular pressure.

Attempts have been made to treat diseases by pharmacologically modulating autophagy activity. Indeed, empagliflozin has been reported to attenuate diabetic tubulopathy by enhancing autophagy [25,26]. However, considering that a HFD activates autophagy and at later stages causes autophagic stagnation, simply inducing autophagy can place a greater burden on the lysosomal system. A compelling aspect of our proposed mechanism is that proper autophagy enhancement against additional stressors could account for the reduced risk of AKI associated with SLC5A2 inhibitors in clinical trials. Moreover, empagliflozin may represent a promising therapeutic approach to other kidney conditions, such as kidney aging, DKD, and phosphate toxicity, in which autophagic stagnation is also observed [22,43,44]. Proximal tubule-specific deletion of Atg5 in mice resulted in significant kidney function deterioration, tubular atrophy, and fibrosis [22,23]. With increasing age, the kidney is

more reliant on autophagy for the removal of damaged proteins and organelles, suggesting that compromised autophagy itself accelerates kidney damage, whereas empagliflozin may protect the kidney from disease progression and slow kidney aging. Thus, empagliflozin may be a safe therapy for elderly CKD patients.

This study has some limitations. First, receptor-mediated ALB reabsorption other than LRP2 was not investigated. In addition to LRP2, CUBN and AMN (amnionless) are involved in ALB reabsorption in PTECs. Lrp2 and CUBN interact for the coordinated uptake of ALB [9], but CUBN-dependent ALB reabsorption is also reported in mice and humans [45,46]. Moreover, AMN plays a role in ALB reabsorption by delivering CUBN to the membrane [47]. Although our study focused on LRP2-mediated ALB reabsorption, CUBN- or AMN-mediated pathways could also be involved in the pathogenesis, which we did not investigate. Second, although empagliflozin reduces the burden on S3 segments as well as S1–2 segments probably because of decreasing glomerular ALB filtration (Figure 5), the mechanisms underlying the reduction in ALB reabsorption remain to be fully elucidated. It is possible that SLC5A2 might have a role in promoting ALB reabsorption in the S1–2 segment, which could explain the results of empagliflozin's suppressing ALB reabsorption in S1–2 segments. There are reports that empagliflozin has direct effects on proximal tubules. For example, one recent paper demonstrates SLC5A2 inhibitors suppress early proximal tubule glucotoxicity and broadly downregulate the apical uptake transport machinery [48].

In conclusion, we describe a novel link between SLC5A2 inhibition, reabsorption of toxic ALB *via* LRP2, and autophagic stagnation in PTECs. Our findings may explain the mechanisms underlying the renoprotective effects of empagliflozin.

Materials and methods

Mice

GFP-MAP1LC3 transgenic, *Atg5^{F/F}*; *NdrG1-CreERT2*, and *Lrp2^{F/F}*; *NdrG1-CreERT2* mice, were used as described previously. [16,22,34,49,50] Eight-week-old mice were fed a normal diet (12.8% of kcal from fat: 5% fat, 23% protein, and 55% carbohydrate; Oriental Yeast, OYC2103800) or HFD (62.2% of kcal from fat: 35% fat, 23% protein, and 25% carbohydrate; Oriental Yeast, OYC 2,900,100) for 2 or 10 months. Empagliflozin (10 mg/kg/day; provided by Boehringer Ingelheim) diluted in 0.5% (w:v) methylcellulose was orally administered. For an IR injury examination, empagliflozin was administered for 2 weeks before ischemia induction. Empagliflozin was administered for 2 weeks before injection of Alexa Fluor 555-conjugated BSA (Invitrogen, A34786). Empagliflozin was administered for 2 weeks before tamoxifen injection for *Atg5* deletion in 5/6 nephrectomized mice. For a long-term examination, empagliflozin was mixed into the HFD at 0.03% (wt:wt). [51] For the induction of *atg5* or *lrp2* deletion, tamoxifen (Sigma-Aldrich, T5648; 1 mg/10 g body wt) dissolved in corn oil (Sigma-Aldrich, C8267) was injected at

a concentration of 10 mg/ml 3 d a week or 2 d a week, respectively. Cilastatin (Wako Pure Chemicals, QA-2867) dissolved in saline was injected at a concentration of 300 mg/kg daily for 7 days before ischemia induction. In the experiment assessing autophagic flux *in vivo*, chloroquine (Sigma-Aldrich, C6628; 50 mg/g body weight) was injected intraperitoneally 6 h before euthanasia. [22] For the study of 5/6 nephrectomized mice, firstly, the upper and lower poles of left side kidney were removed with the adrenal gland reserved. Seven days later, the right side of kidney was fully removed. Sham control mice were subjected to the same surgical procedures at the same time. [31] Kidney ischemia was induced, and tubular injury and kidney functions were assessed, as described previously. [16] All animal experiments were approved by the Animal Research Committee of Osaka University (01-042-018) and conformed to the Japanese Animal Protection and Management Law (No.25).

Antibodies and reagents

We used the following antibodies; LRP2/MEGALIN (gifted by Dr. Michigami, Department of Bone and Mineral Research, Osaka Medical Center and Research Institute for Maternal and Child Health, Japan, or BiCell Scientific 31,012), COL1A1 (Abcam, ab34710), SQSTM1/p62 (Medical and Biological Laboratory [MBL], PM045 for western blotting, Progen, GP62C for immunostaining), ubiquitin (Cell Signaling Technology, 3936), ATG5 (MBL, PM050), MAP1LC3 (Cell Signaling Technology, 2755 for western blotting, MBL, PM036 for immunostaining), ACTB (Sigma-Aldrich, A5316), ADGRE1/F4/80 (BIO-RAD, MCA497), CTSD (CST 31,718), CTSD (CST 88,239), LAMP1 (BD Biosciences 553,792), 4HNE (Japan Institute for the Control of Aging, MHN-020P), DT (Japan Institute for the Control of Aging, MDT-020P), PSMA7/proteasome 20S α 6 (abcam, ab22673), HAVCR1/KIM1 (R&D Systems, AF1750), SLC5A2/SGLT2 (Abcam, ab85626), RBP (Dako, A0040), GC/VDP (Novus Biologicals, NBP1–88027), biotinylated secondary antibodies (Vector Laboratories, BA-1000 [anti-rabbit IgG], BA-2001 [anti-mouse IgG], BA-4000 [anti-rat IgG], BA-7000 [anti-guinea pig IgG]), horseradish peroxidase-conjugated secondary antibodies (DAKO, P0448 [anti-rabbit IgG], P0447 [anti-mouse IgG], and P0450 [anti-rat IgG]), and Alexa Fluor-conjugated secondary antibody (Invitrogen, A11034 [anti-rabbit Alexa Fluor 488], A11006 [anti-rat Alexa Fluor 488], A27039 [anti-rabbit Alexa Fluor 555], and A21247 [anti-rat Alexa Fluor 647]).

Histological analysis

Histological analysis was performed as described previously with modifications. [16] For evaluation of PAS-stained sections, tubular vacuolation was graded semiquantitatively from 0 to 10 according to the percentage of vacuolated tubules. [17] Antigen retrieval on paraffin-embedded sections, double staining for SQSTM1/p62 (ubiquitin or LAMP1) and LRP2/MEGALIN, quantification of the percentage of the COL1A1 (or ADGRE1/F4/80)-positive area,

electron microscopy analysis, toluidine blue and Nile red staining, and assessment of the kidney injury were performed as described previously. [16,52] TUNEL staining was performed using the ApopTag Peroxidase *In Situ* Apoptosis Detection Kit (EMD Millipore Corporation, S7100). Masson's trichrome staining was performed using a standard procedure.

Biochemical parameters

Blood samples were collected from mice under anesthesia. Plasma was obtained after centrifugation (15 min, 845 × g, 4°C) and concentrations of cystatin C, creatinine, urea nitrogen, glucose, total cholesterol, TGs, and phospholipids were measured using the cystatin C (mouse) ELISA kit (BioVendor, RD291009200R), QuantiChrom™ Creatinine Assay Kit (DICT-500), BUN-Test-Wako (Wako, 279-36201), Glucose CII-test (Wako, 439-90901), Cholesterol E-test (Wako, 439-17501), Triglyceride E-test (Wako, 432-40201), and Phospholipid C-test (Wako, 433-36201), respectively. All kits were used in accordance with the manufacturer's instructions.

Measurement of 24 free fatty acid fractions

The serum levels of 24 FA fractions were measured as per a method described previously (The Japan Institute for the Control of Aging). [53] In brief, serum lipids were extracted using Folch procedure. [54] Next, using tricosanoic acid (C23:0) as an internal standard, fatty acids were methylated using boron trifluoride and methanol, and the methylated fatty acids were analyzed using a capillary gas chromatograph (GC-2010; Shimadzu Corporation) and a BPX70 capillary column (0.25 mm ID 30 m; SGE International Ltd).

Analyses of ALB reabsorption in proximal tubules

To investigate renal reabsorption of glomerular-filtered ALB, mice were intravenously injected with Alexa Fluor 555-conjugated BSA (10 µg/kg body wt, dissolved in 0.1 ml of phosphate-buffered saline (pH 7.4; composed of 137 mm NaCl [Wako, 191-01665], 8 mm Na₂HPO₄ [Wako, 196-02835], 2.7 mm KCl [Nacalai tesque 28,514-75], 1.5 mm KH₂PO₄ [Wako, 169-04245]). Ten minutes after injection, mice were briefly perfused with phosphate-buffered saline, and the left kidney was removed and fixed with 4% PFA. Kidney sections were then stained with LRP2/MEGALIN or SLC5A2/SGLT2, and images were acquired by confocal microscopy (FV1200; Olympus)

Measurement of urinary ALB

Urine samples were collected over the course of 24 h using metabolic cages in which mice were able to freely access food and water. Collected urine samples were centrifuged to remove debris. Clear supernatants of urine samples were used to measure ALB concentrations using a Mouse Albumin ELISA Kit (Bethyl Laboratories, E99-134) according

to the manufacturer's instructions. Urinary ALB levels are reported as 24 h urinary ALB for 24 h urine.

Quantitative RT-PCR and Western blot analysis

Quantitative RT-PCR and western blot analyses were performed as per a method described previously. [55] The sequences of the primers used, except *Lrp2*, have been described previously. [22,52,56] The sequences of the *Lrp2* primer were as follows: *Lrp2*-F, 5'-tgcccaagctgccaagct-3'; *Lrp2*-R, 5'-cacaccgatgtccatgttcaca-3'.

Multiphoton In Vivo Imaging

The animals were anesthetized with an intraperitoneal injection of medetomidine, midazolam, and butorphanol. A catheter was inserted into the right carotid artery for reagent infusion. The left kidney was exteriorized through a flank incision and the animal placed on a cover glass. The microscope stage had a heater to keep the body temperature at 36–38°C. Another heater maintained the temperature inside the microscope cover at 36–38°C. The images were acquired using a Nikon A1R-MP multiphoton microscopy (Japan) equipped with a ×20 water-immersion objective lens. Multiphoton imaging was used with 820-nm laser excitation and detection of lucifer yellow (LY; Invitrogen, L453) through 593/46 nm bandpass filters. LY was injected in bolus to measure SNGFR (20 µl of a 100 µg/ml stock in intravenous bolus).

Measurement of SNGFR

After detecting a superficial glomerulus and subsequent proximal tubule that could be observed for a minimum optical section of 100 µm, the freely filtered LY was injected into the carotid artery, and transit of filtered LY downstream of the proximal tubule was visualized. SNGFR was calculated by measuring the fluorescence intensity change of LY within 2 regions of interest (ROIs) ≈ 100 to 200 µm apart in the early proximal tubule segment, internal diameter, and length of the tubule. $SNGFR = [\text{tubular fluid volume}]/[\text{transit time of filtrate}]$, $[\text{tubular fluid volume}] = [\text{length of between the two ROIs} \times (\text{internal diameter}/2)^2 \times \pi]$, $[\text{transit time of filtrate}] = \text{LY transit time between the two ROIs}$, which was calculated at the peak of each ROIs. Images were collected in a time (*xyt*, 60 Hz) series.

Statistical analysis

All results have been presented as means ± standard error (SE). Statistical analyses were conducted using the JMP software (SAS Institute). Multiple-group comparisons were performed using analysis of variance with post-testing using the Tukey-Kramer test. The difference between two experimental values was assessed using the Student's *t*-test when appropriate. Statistical significance was defined as $p < 0.05$.

Acknowledgements

We thank N. Mizushima at the University of Tokyo, for the *Atg5^{F/F}* and GFP-MAP1LC3 mice; Keita P. Mori and Hideki Yokoi at the Kyoto

University Graduate School of Medicine and Kiyoshi Mori at the Shizuoka General Hospital for the *Lrp2^{F/F}* mice; T. Michigami at the Osaka Medical Center and Research Institute for the LRP2/MEGALIN antibody; Kengo Kidokoro at the Kawasaki Medical School for the method of in vivo imaging to measure SNGFR, and N. Horimoto for technical assistance. We are also grateful to the Nikon Imaging Center at Osaka University for their assistance with multiphoton microscopy, image acquisition, and analysis.

Disclosure statement

This study was supported by Boehringer Ingelheim (Ingelheim am Rheine, Germany) and Nippon Boehringer Ingelheim (Tokyo, Japan) through a Material Transfer Agreement. Boehringer Ingelheim had no role in the design, analysis, or interpretation of the results in this study. Boehringer Ingelheim was given the opportunity to review the manuscript for medical and scientific accuracy as it relates to Boehringer Ingelheim substances, as well as intellectual property considerations.

Funding

This work was supported by a Grant-in-Aid for Scientific Research from the Ministry of Education, Culture, Sports, Science, and Technology in Japan (17K16083 and 21K16163 [to T.Y.] and 21H02935 [to Y.I.]), MSD Life Science Foundation, and the Ichiro Kanehara Foundation (to T.Y.). Part of this study was financially supported by Nippon Boehringer Ingelheim Co., Ltd. as a collaboration study.

Abbreviations

4-HNE	4-hydroxy-2-nonenal
ACTB	actin, beta
ADGRE1/F4/80	adhesion G protein-coupled receptor E1
AKI	acute kidney injury
ATG	autophagy related
BSA	bovine serum albumin
CKD	chronic kidney disease
COL1A1	collagen, type I, alpha 1
CTSB	cathepsin B
CTSD	cathepsin D
DT	dityrosine
DKD	diabetic kidney disease
ESRD	end-stage renal disease
FA	fatty acid
GAPDH	glyceraldehyde-3-phosphate dehydrogenase
GFP	green fluorescent protein
HFD	high-fat diet
HAVCR1/KIM1	hepatitis A virus cellular receptor 1
iAtg5KO	inducible <i>atg5</i> knockout
iLrp2KO	inducible <i>lrp2/Megalin</i> knockout
IR	ischemia-reperfusion
LAMP1	lysosomal-associated membrane protein 1
LRP2/megalin	low density lipoprotein receptor-related protein 2
MAP1LC3B/LC3	microtubule-associated protein 1 light chain 3 beta
ND	normal diet
PAS	periodic-acid schiff
PTEC	proximal tubular epithelial cell
PUFA	polyunsaturated fatty acids
RAAS	Renin-angiotensin-aldosterone system
SLC5A2/SGLT2	solute carrier family 5 (sodium/glucose cotransporter), member 2
SNGFR	single nephron glomerular filtration rate
SQSTM1/p62	sequestosome 1
TUNEL	terminal deoxynucleotidyl transferase dUTP nick end labeling

References

- [1] Kovesdy CP. Epidemiology of chronic kidney disease: an update 2022. *Kidney Int Suppl.* 2022 Apr;12(1):7–11. doi: 10.1016/j.kisu.2021.11.003
- [2] Wanner C, Inzucchi SE, Lachin JM, et al. Empagliflozin and progression of kidney disease in type 2 diabetes. *N Engl J Med.* [2016 Jul 28];375(4):323–334. doi: 10.1056/NEJMoa1515920
- [3] Neuen BL, Young T, Heerspink HJL, et al. SGLT2 inhibitors for the prevention of kidney failure in patients with type 2 diabetes: a systematic review and meta-analysis. *Lancet Diabetes & Endocrinol.* 2019;7(11):845–854. doi: 10.1016/S2213-8587(19)30256-6
- [4] Baigent C, Emberson J, Haynes R, et al. Impact of diabetes on the effects of sodium glucose co-transporter-2 inhibitors on kidney outcomes: collaborative meta-analysis of large placebo-controlled trials. *Lancet.* 2022;400(10365):1788–1801. doi: 10.1016/S0140-6736(22)02074-8
- [5] Heerspink HJL, Stefansson BV, Correa-Rotter R, et al. Dapagliflozin in patients with chronic kidney disease. *N Engl J Med.* [2020 Oct 8];383(15):1436–1446. doi: 10.1056/NEJMoa2024816
- [6] Herrington WG, Staplin N, Wanner C, et al. Empagliflozin in patients with chronic kidney disease. *N Engl J Med.* [2023 Jan 12];388(2):117–127.
- [7] Cherney DZ, Perkins BA, Soleymanlou N, et al. Renal hemodynamic effect of sodium-glucose cotransporter 2 inhibition in patients with type 1 diabetes mellitus. *Circulation.* [2014 Feb 4];129(5):587–597. doi: 10.1161/CIRCULATIONAHA.113.005081
- [8] Kidokoro K, Cherney DZI, Bozovic A, et al. Evaluation of glomerular hemodynamic function by Empagliflozin in diabetic mice using in vivo imaging. *Circulation.* [2019 Jul 23];140(4):303–315. doi: 10.1161/CIRCULATIONAHA.118.037418
- [9] Nielsen R, Christensen EI, Birn H. Megalin and cubilin in proximal tubule protein reabsorption: from experimental models to human disease. *Kidney Int.* 2016 Jan;89(1):58–67. doi: 10.1016/j.kint.2015.11.007
- [10] Dickson LE, Wagner MC, Sandoval RM, et al. The proximal tubule and albuminuria: really! *J Am Soc Nephrol.* 2014 Mar;25(3):443–453. doi: 10.1681/ASN.2013090950
- [11] Birn H, Nielsen R, Weyer K. Tubular albumin uptake: is there evidence for a quantitatively important, receptor-independent mechanism? *Kidney Int.* 2023 Dec;104(6):1069–1073. doi: 10.1016/j.kint.2023.07.030
- [12] Tenten V, Menzel S, Kunter U, et al. Albumin is recycled from the primary urine by tubular transcytosis. *J Am Soc Nephrol.* 2013 Dec;24(12):1966–1980. doi: 10.1681/ASN.2013010018
- [13] Tojo A. The role of the kidney in protein metabolism: the capacity of tubular lysosomal proteolysis in nephrotic syndrome. *Kidney Int.* 2013 Nov;84(5):861–863. doi: 10.1038/ki.2013.284
- [14] Christensen EI, Kristoffersen IB, Grann B, et al. A well-developed endolysosomal system reflects protein reabsorption in segment 1 and 2 of rat proximal tubules. *Kidney Int.* 2021 Apr;99(4):841–853. doi: 10.1016/j.kint.2020.11.015
- [15] Takahashi A, Takabatake Y, Kimura T, et al. Autophagy inhibits the accumulation of advanced glycation end products by promoting lysosomal biogenesis and function in the kidney proximal tubules. *Diabetes.* 2017 May;66(5):1359–1372. doi: 10.2337/db16-0397
- [16] Yamamoto T, Takabatake Y, Takahashi A, et al. High-fat diet-induced lysosomal dysfunction and impaired autophagic flux contribute to Lipotoxicity in the kidney. *J Am Soc Nephrol.* 2017 May;28(5):1534–1551. doi: 10.1681/ASN.2016070731
- [17] Nakamura J, Yamamoto T, Takabatake Y, et al. Tfeb-mediated lysosomal exocytosis alleviates high-fat diet-induced lipotoxicity in the kidney. *JCI Insight.* [2023 Feb 22];8(4). doi: 10.1172/jci.insight.162498
- [18] Baines RJ, Brunskill NJ. Tubular toxicity of proteinuria. *Nat Rev Nephrol.* 2011 Mar;7(3):177–180. doi: 10.1038/nrneph.2010.174
- [19] Makhammajanov Z, Gaipov A, Myngbay A, et al. Tubular toxicity of proteinuria and the progression of chronic kidney disease.

- Nephrol Dial Transplant. [2023 Oct 3];39(4):589–599. doi: [10.1093/ndt/gfad215](https://doi.org/10.1093/ndt/gfad215)
- [20] Mizushima N, Levine B, Longo DL. Autophagy in human diseases. *N Engl J Med*. [2020 Oct 15];383(16):1564–1576. doi: [10.1056/NEJMra2022774](https://doi.org/10.1056/NEJMra2022774)
- [21] Takabatake Y, Yamamoto T, Isaka Y. Stagnation of autophagy: a novel mechanism of renal lipotoxicity. *Autophagy*. [2017 Apr 3];13(4):775–776. doi: [10.1080/15548627.2017.1283084](https://doi.org/10.1080/15548627.2017.1283084)
- [22] Yamamoto T, Takabatake Y, Kimura T, et al. Time-dependent dysregulation of autophagy: implications in aging and mitochondrial homeostasis in the kidney proximal tubule. *Autophagy*. [2016 May 3];12(5):801–813. doi: [10.1080/15548627.2016.1159376](https://doi.org/10.1080/15548627.2016.1159376)
- [23] Minami S, Sakai S, Yamamoto T, et al. FGF21 and autophagy coordinately counteract kidney disease progression during aging and obesity. *Autophagy*. 2023 Sep;20(3):1–16. doi: [10.1080/15548627.2023.2259282](https://doi.org/10.1080/15548627.2023.2259282)
- [24] Bordi M, Berg MJ, Mohan PS, et al. Autophagy flux in CA1 neurons of alzheimer hippocampus: increased induction overburdens failing lysosomes to propel neuritic dystrophy. *Autophagy*. 2016 Dec;12(12):2467–2483. doi: [10.1080/15548627.2016.1239003](https://doi.org/10.1080/15548627.2016.1239003)
- [25] Lee YH, Kim SH, Kang JM, et al. Empagliflozin attenuates diabetic tubulopathy by improving mitochondrial fragmentation and autophagy. *Am J Physiol Renal Physiol*. [2019 Oct 1];317(4):F767–F780. doi: [10.1152/ajprenal.00565.2018](https://doi.org/10.1152/ajprenal.00565.2018)
- [26] Ala M, Khoshdel MRF, Dehpour AR, et al. Empagliflozin enhances autophagy, mitochondrial biogenesis, and antioxidant defense and ameliorates renal Ischemia/Reperfusion in nondiabetic rats. *Oxid Med Cell Longev*. 2022;2022:1–9. doi: [10.1155/2022/1197061](https://doi.org/10.1155/2022/1197061)
- [27] Brown WJ, Sullivan TR, Greenspan P. Nile red staining of lysosomal phospholipid inclusions. *Histochemistry*. 1992 May;97(4):349–354. doi: [10.1007/BF00270037](https://doi.org/10.1007/BF00270037)
- [28] Humanes B, Lazaro A, Camano S, et al. Cilastatin protects against cisplatin-induced nephrotoxicity without compromising its anticancer efficiency in rats. *Kidney Int*. 2012 Sep;82(6):652–663. doi: [10.1038/ki.2012.199](https://doi.org/10.1038/ki.2012.199)
- [29] Hori Y, Aoki N, Kuwahara S, et al. Megalin blockade with cilastatin suppresses drug-induced nephrotoxicity. *J Am Soc Nephrol*. 2017 Jun;28(6):1783–1791. doi: [10.1681/ASN.2016060606](https://doi.org/10.1681/ASN.2016060606)
- [30] Kuwahara S, Hosojima M, Kaneko R, et al. Megalin-mediated Tubuloglomerular alterations in high-fat diet-induced kidney disease. *J Am Soc Nephrol*. 2016 Jul;27(7):1996–2008. doi: [10.1681/ASN.2015020190](https://doi.org/10.1681/ASN.2015020190)
- [31] Gong W, Mao S, Yu J, et al. NLRP3 deletion protects against renal fibrosis and attenuates mitochondrial abnormality in mouse with 5/6 nephrectomy. *Am J Physiol Renal Physiol*. [2016 May 15];310(10):F1081–8. doi: [10.1152/ajprenal.00534.2015](https://doi.org/10.1152/ajprenal.00534.2015)
- [32] Vallon V, Thomson SC. The tubular hypothesis of nephron filtration and diabetic kidney disease. *Nat Rev Nephrol*. 2020 Jun;16(6):317–336. doi: [10.1038/s41581-020-0256-y](https://doi.org/10.1038/s41581-020-0256-y)
- [33] Deji N, Kume S, Araki S, et al. Structural and functional changes in the kidneys of high-fat diet-induced obese mice. *Am J Physiol Renal Physiol*. 2009 Jan;296(1):F118–26. doi: [10.1152/ajprenal.00110.2008](https://doi.org/10.1152/ajprenal.00110.2008)
- [34] Mori KP, Yokoi H, Kasahara M, et al. Increase of total nephron albumin filtration and reabsorption in diabetic nephropathy. *J Am Soc Nephrol*. 2017 Jan;28(1):278–289. doi: [10.1681/ASN.2015101168](https://doi.org/10.1681/ASN.2015101168)
- [35] Innes JK, Calder PC. Marine omega-3 (N-3) fatty acids for cardiovascular health: an update for 2020. *Int J Mol Sci*. [2020 Feb 18];21(4):1362. doi: [10.3390/ijms21041362](https://doi.org/10.3390/ijms21041362)
- [36] Theilig F, Kriz W, Jerichow T, et al. Abrogation of protein uptake through megalin-deficient proximal tubules does not safeguard against tubulointerstitial injury. *J Am Soc Nephrol*. 2007 Jun;18(6):1824–1834. doi: [10.1681/ASN.2006111266](https://doi.org/10.1681/ASN.2006111266)
- [37] Mahadevappa R, Nielsen R, Christensen EI, et al. Megalin in acute kidney injury: foe and friend. *Am J Physiol Renal Physiol*. 2014 Jan;306(2):F147–54. doi: [10.1152/ajprenal.00378.2013](https://doi.org/10.1152/ajprenal.00378.2013)
- [38] Motoyoshi Y, Matsusaka T, Saito A, et al. Megalin contributes to the early injury of proximal tubule cells during nonselective proteinuria. *Kidney Int*. 2008 Nov;74(10):1262–1269. doi: [10.1038/ki.2008.405](https://doi.org/10.1038/ki.2008.405)
- [39] Liu D, Wen Y, Tang TT, et al. Megalin/cubulin-lysosome-mediated albumin reabsorption is involved in the tubular cell activation of NLRP3 inflammasome and tubulointerstitial inflammation. *J Biol Chem*. [2015 May 29];290(29):18018–18028. doi: [10.1074/jbc.M115.662064](https://doi.org/10.1074/jbc.M115.662064)
- [40] Peruchetti DB, Barahuna-Filho PFR, Silva-Aguiar RP, et al. Megalin-mediated albumin endocytosis in renal proximal tubules is involved in the antiproteinuric effect of angiotensin II type 1 receptor blocker in a subclinical acute kidney injury animal model. *Biochim et Biophys Acta (BBA) - Gener Subj*. 2021;1865(9):129950. doi: [10.1016/j.bbagen.2021.129950](https://doi.org/10.1016/j.bbagen.2021.129950)
- [41] Janssens V, Gaide Chevronnay HP, Marie S, et al. Protection of cystinotic mice by kidney-specific megalin ablation supports an endocytosis-based mechanism for nephropathic cystinosis progression. *J Am Soc Nephrol*. [2019 Sep 23];30(11):2177–2190. doi: [10.1681/ASN.2019040371](https://doi.org/10.1681/ASN.2019040371)
- [42] Matsushita K, Mori K, Saritas T, et al. Cilastatin ameliorates Rhabdomyolysis-induced AKI in mice. *J Am Soc Nephrol*. 2021 Oct;32(10):2579–2594. doi: [10.1681/ASN.2020030263](https://doi.org/10.1681/ASN.2020030263)
- [43] Sakai S, Yamamoto T, Takabatake Y, et al. Proximal tubule autophagy differs in type 1 and 2 diabetes. *J Am Soc Nephrol*. 2019 Jun;30(6):929–945. doi: [10.1681/ASN.2018100983](https://doi.org/10.1681/ASN.2018100983)
- [44] Fujimura R, Yamamoto T, Takabatake Y, et al. Autophagy protects kidney from phosphate-induced mitochondrial injury. *Biochem Biophys Res Commun*. [2020 Apr 9];524(3):636–642. doi: [10.1016/j.bbrc.2020.01.137](https://doi.org/10.1016/j.bbrc.2020.01.137)
- [45] Weyer K, Storm T, Shan J, et al. Mouse model of proximal tubule endocytic dysfunction. *Nephrol Dial Transplant*. 2011 Nov;26(11):3446–3451. doi: [10.1093/ndt/gfr525](https://doi.org/10.1093/ndt/gfr525)
- [46] Bedin M, Boyer O, Servais A, et al. Human C-terminal CUBN variants associate with chronic proteinuria and normal renal function. *J Clin Invest*. [2020 Jan 2];130(1):335–344. doi: [10.1172/JCI129937](https://doi.org/10.1172/JCI129937)
- [47] Ahuja R, Yammani R, Bauer JA, et al. Interactions of cubilin with megalin and the product of the amnionless gene (AMN): effect on its stability. *Biochem J*. [2008 Mar 1];410(2):301–308. doi: [10.1042/BJ20070919](https://doi.org/10.1042/BJ20070919)
- [48] Billing AM, Kim YC, Gullaksen S, et al. Metabolic communication by SGLT2 inhibition. *Circulation*. [2024 Mar 12];149(11):860–884. doi: [10.1161/CIRCULATIONAHA.123.065517](https://doi.org/10.1161/CIRCULATIONAHA.123.065517)
- [49] Leheste JR, Melsen F, Wellner M, et al. Hypocalcemia and osteopathy in mice with kidney-specific megalin gene defect. *Faseb J*. 2003 Feb;17(2):247–249. doi: [10.1096/fj.02-0578fj](https://doi.org/10.1096/fj.02-0578fj)
- [50] Endo T, Nakamura J, Sato Y, et al. Exploring the origin and limitations of kidney regeneration. *J Pathol*. 2015 Jun;236(2):251–263. doi: [10.1002/path.4514](https://doi.org/10.1002/path.4514)
- [51] Xu L, Nagata N, Nagashimada M, et al. SGLT2 inhibition by empagliflozin promotes fat utilization and Browning and attenuates inflammation and insulin resistance by polarizing M2 macrophages in diet-induced obese mice. *EBioMedicine*. 2017 Jun;20:137–149. doi: [10.1016/j.ebiom.2017.05.028](https://doi.org/10.1016/j.ebiom.2017.05.028)
- [52] Yamamoto T, Takabatake Y, Minami S, et al. Eicosapentaenoic acid attenuates renal lipotoxicity by restoring autophagic flux. *Autophagy*. 2021 Jul;17(7):1700–1713. doi: [10.1080/15548627.2020.1782034](https://doi.org/10.1080/15548627.2020.1782034)
- [53] Nozue T, Yamamoto S, Tohyama S, et al. Effects of statins on serum n-3 to n-6 polyunsaturated fatty acid ratios in patients with coronary artery disease. *J Cardiovasc Pharmacol Ther*. 2013 Jul;18(4):320–326. doi: [10.1177/1074248412473202](https://doi.org/10.1177/1074248412473202)
- [54] Folch J, Lees M, Sloane Stanley GH. A simple method for the isolation and purification of total lipides from animal tissues. *J Biol Chem*. 1957 May;226(1):497–509. doi: [10.1016/S0021-9258\(18\)64849-5](https://doi.org/10.1016/S0021-9258(18)64849-5)
- [55] Matsui I, Ito T, Kurihara H, et al. Snail, a transcriptional regulator, represses nephrin expression in glomerular epithelial cells of nephrotic rats. *Lab Invest*. 2007 Mar;87(3):273–283. doi: [10.1038/labinvest.3700518](https://doi.org/10.1038/labinvest.3700518)
- [56] Minami S, Yamamoto T, Takabatake Y, et al. Lipophagy maintains energy homeostasis in the kidney proximal tubule during prolonged starvation. *Autophagy*. [2017 Oct 3];13(10):1629–1647. doi: [10.1080/15548627.2017.1341464](https://doi.org/10.1080/15548627.2017.1341464)